

# Journal of Biomedical Optics

[SPIEDigitalLibrary.org/jbo](http://SPIEDigitalLibrary.org/jbo)

## **Visualization of peripheral vasodilative indices in human skin by use of red, green, blue images**

Izumi Nishidate  
Noriyuki Tanaka  
Tatsuya Kawase  
Takaaki Maeda  
Tomonori Yuasa  
Yoshihisa Aizu  
Tetsuya Yuasa  
Kyuichi Niizeki

# Visualization of peripheral vasodilative indices in human skin by use of red, green, blue images

Izumi Nishidate,<sup>a</sup> Noriyuki Tanaka,<sup>a</sup> Tatsuya Kawase,<sup>a</sup> Takaaki Maeda,<sup>b</sup> Tomonori Yuasa,<sup>c</sup> Yoshihisa Aizu,<sup>c</sup> Tetsuya Yuasa,<sup>d</sup> and Kyuichi Niizeki<sup>d</sup>

<sup>a</sup>Tokyo University of Agriculture and Technology, Graduate School of Bio-application and Systems Engineering, Koganei, Tokyo 184-8588, Japan

<sup>b</sup>Kushiro National College of Technology, Department of Mechanical Engineering, Kushiro, Hokkaido 084-0916, Japan

<sup>c</sup>Muroran Institute of Technology, College of Design and Manufacturing Technology, Muroran, Hokkaido 050-8588, Japan

<sup>d</sup>Yamagata University, Graduate School of Biosystem Engineering, Yonezawa, Yamagata 992-8510, Japan

**Abstract.** We propose a method to visualize the arterial inflow, the vascular resistance, and the venous capacitance in the skin tissue from red, green, blue (RGB) digital color images. The arterial inflow and the venous capacitance in the skin tissue are visualized based on an increase in the rate of change in the total blood concentration and the change of the total blood concentration during upper limb occlusion at a pressure of 50 mmHg. The resultant arterial inflow with the measured mean arterial pressure also provides an image of the vascular resistance in human skin. The arterial inflow, the vascular resistance, and the venous capacitance acquired by the method are well correlated with those obtained from the conventional strain-gauge plethysmograph. The correlation coefficients  $R$  between the estimated values by the method and the measurements by the SPG are calculated to be 0.83 ( $P < 0.001$ ) for the arterial inflow, 0.77 ( $P < 0.01$ ) for the vascular resistance, and 0.77 ( $P < 0.01$ ) for the venous capacitance. The arterial inflow and the venous capacitance in the skin tissue are significantly higher in active subjects compared with the sedentary subjects, whereas the vascular resistance was significantly lower in the active subjects compared with the sedentary subjects. The results of the present study indicate the possibility of using the proposed method for evaluating the peripheral vascular functions in human skin. © 2012 Society of Photo-Optical Instrumentation Engineers (SPIE). [DOI: 10.1117/1.JBO.18.6.061220]

Keywords: arterial inflow; vascular resistance; venous capacitance; skin hemodynamics; RGB image; Monte Carlo simulation; strain-gauge plethysmograph; upper arm occlusion.

Paper 12578SSP received Sep. 5, 2012; revised manuscript received Nov. 18, 2012; accepted for publication Nov. 19, 2012; published online Dec. 17, 2012.

## 1 Introduction

Quantitative evaluation of the peripheral hemodynamics is important for clinical and physiological assessments of vascular functions. Impaired vasodilatation is associated with most forms of cardiovascular disease, such as hypertension, coronary artery disease, chronic heart failure, peripheral artery disease, diabetes, and chronic renal failure,<sup>1</sup> as well as a lack of physical activity due to spinal cord injury or a sedentary lifestyle.<sup>2-4</sup> Therefore early detection of impaired vasodilatation is useful as a prognostic of disease progression in various vascular dysfunctions. The strain-gauge plethysmograph (SPG) has been widely used to evaluate vasodilatation based on hemodynamics.<sup>5-8</sup> The SPG is a device that measures the volume changes in limbs and digits by using a gauge made of a mercury-filled silastic rubber tube. The volume change of tissue induced by the flow of blood, mainly through skeletal muscle, but also through skin and bone, stretches and contracts the gauge.<sup>9,10</sup> By using the SPG, several indices of arterial and venous functions related to vasodilatation—such as arterial inflow, peripheral vascular resistance, and venous capacitance—can be calculated from the changes in limb volume due to the changes in blood flow.<sup>2,3,11-13</sup> Arterial inflow is calculated from an increase in the rate of change in blood volume immediately after venous

occlusion, and it reflects the arterial contribution to vasodilatation. Vascular resistance can be calculated by dividing the mean arterial pressure by the arterial inflow. The assessment of vascular resistance has been performed for patients with spinal cord injury<sup>2</sup> and for hypertensive patients<sup>11,12</sup> based on the arterial inflow measured by the SPG. On the other hand, venous capacitance is the term used to describe the ability of the veins to stretch, and it is given as the change in blood volume after venous occlusion. The SPG recording demonstrated that venous capacitance is significantly less in diabetic patients than in non-diabetic subjects.<sup>13</sup> It was also lower in patients with spinal cord injury than in able-bodied subjects and in sedentary subjects compared with the active-lifestyle subjects.<sup>3</sup> Although the SPG has been used to investigate the vascular functions as mentioned above, it often suffers from errors due to limb movement because the mercury rubber strain-gauge is directly attached to the area being measured. Moreover, the measurements are usually limited to limbs and digits.

Laser-Doppler blood flowmetry has also been employed to measure the cutaneous blood perfusion for evaluating peripheral vascular function.<sup>4,14,15</sup> Both arterial inflow and venous capacitance have been estimated from the cutaneous blood flow by using a laser-Doppler system to investigate the influence of physical activity on the response to leg compression.<sup>4</sup> Combinations of laser-Doppler flowmetry and iontophoresis of tissue-simulating drugs have been performed to measure the cutaneous

Address all correspondence to: Izumi Nishidate, Tokyo University of Agriculture and Technology, Graduate School of Bio-application and Systems Engineering, Koganei, Tokyo 184-8588, Japan. Tel: +81-42-388-7065; Fax: +81-42-388-7065; E-mail: [inishi@cc.tuat.ac.jp](mailto:inishi@cc.tuat.ac.jp)

blood perfusion for the evaluation of endothelium-mediated vasodilatation.<sup>14,15</sup> Although laser-Doppler flowmetry has been used in many applications, its inability to be implemented clinically can be attributed to its high cost and low spatial and temporal resolutions when investigating large areas.

Diffuse reflectance spectroscopy (DRS) has been widely used for the evaluation of human skin chromophores.<sup>16-25</sup> The multispectral imaging technique is a useful tool for extending DRS to the spatial mapping of the chromophores in skin tissue. This can be simply achieved by a monochromatic charge-coupled device (CCD) camera with narrowband filters and a white light source, which has been used to investigate the hemoglobin perfusion in living tissue.<sup>26-28</sup> In clinical conditions, simpler, more cost-effective, and more portable equipment is needed. The digital RGB imaging technique is a promising tool for satisfying these demands for practical application. Imaging with broadband filters, as in the case of digital RGB imaging, can also provide spectral images without mechanical rotation of a filter wheel. Several approaches have been reported for visualizing the concentration of skin chromophores and the subsurface microcirculation of skin by a digital RGB camera.<sup>29-31</sup> We have previously proposed a method by which to visualize the concentrations of melanin, oxygenated blood, and deoxygenated blood distributed in the skin tissue using a digital RGB image.<sup>32</sup> In this method, the RGB values are converted into the tristimulus values in the Commission Internationale de l'Éclairage XYZ (CIEXYZ) color space, which is compatible with the common RGB working space of the National Television Standards Committee (NTSC), the standard RGB (sRGB), etc. A Monte Carlo simulation (MCS) of light transport for the human skin model is used to specify the relationship among the tristimulus XYZ values and the concentrations of melanin, oxygenated blood, and deoxygenated blood. Images of total blood concentration and oxygen saturation can also be reconstructed from the results of oxygenated blood and deoxygenated blood. Using this method, the concentrations of chromophores and tissue oxygen saturation in the skin of the human hand have been investigated for healthy adult subjects during upper limb occlusion at pressures of 50 and 250 mmHg.<sup>33</sup>

In the present study, we newly propose a method to visualize the vasodilative indices of the arterial inflow, the vascular resistance, and the venous capacitance in the skin tissue based on the previously developed technique.<sup>32,33</sup> The arterial inflow and the venous capacitance in the skin tissue are visualized from the increase in the rate of change in the total blood concentration and the change of the total blood concentration during upper limb occlusion at a pressure of 50 mmHg. The resultant arterial inflow with the measured mean arterial pressure provides the image of vascular resistance in human skin. The proposed method based on DRS has the advantage of using a standard digital RGB camera, thus providing a low-cost imaging system with high spatial and temporal resolutions for evaluating the peripheral hemodynamics. In order to confirm the feasibility of the method to evaluate peripheral vascular function in human skin, *in vivo* experiments are performed for subjects with active and sedentary lifestyles during upper limb venous occlusion at a pressure of 50 mmHg. The vasodilative indices obtained from the proposed method are compared with those measured by a conventional SPG. The principal goal of this work is the investigation of a more cost-effective imaging solution of peripheral vasodilative indices in human skin.

## 2 Principle

### 2.1 Relationship Between RGB Values and Skin Chromophore Concentrations

RGB values of a pixel on a skin surface image acquired by a digital camera can be expressed as

$$\begin{bmatrix} R \\ G \\ B \end{bmatrix} = \mathbf{L}_1 \begin{bmatrix} X \\ Y \\ Z \end{bmatrix}, \quad (1)$$

where  $X$ ,  $Y$ , and  $Z$  are the tristimulus values in the CIEXYZ color system and are defined as

$$X = k \sum E(\lambda) \bar{x}(\lambda) O(\lambda), \quad (2)$$

$$Y = k \sum E(\lambda) \bar{y}(\lambda) O(\lambda), \quad (3)$$

$$Z = k \sum E(\lambda) \bar{z}(\lambda) O(\lambda). \quad (4)$$

$\mathbf{L}_1$  is a transformation matrix to convert XYZ values to the corresponding RGB values and exists for each working space (NTSC, PAL/SECAM, sRGB, etc.). In addition,  $\lambda$ ,  $E(\lambda)$ , and  $O(\lambda)$  are the wavelength, the spectral distribution of the illuminant, and the diffuse reflectance spectrum of human skin, respectively, and  $\bar{x}(\lambda)$ ,  $\bar{y}(\lambda)$ , and  $\bar{z}(\lambda)$  are the color matching functions in the CIEXYZ color system. The value of constant  $k$  that results in  $Y$  being equal to 100 for the perfect diffuser is given by

$$k = 100 / \sum E(\lambda) \bar{y}(\lambda). \quad (5)$$

In Eqs. (2) through (5), the summation can be carried out using data at 10-nm intervals, from 400 to 700 nm. Assuming that the skin tissue consists primarily of the stratum corneum, epidermis containing melanin, and dermis containing oxygenated and deoxygenated blood, the diffuse reflectance of skin tissue  $O$  can be expressed as

$$\begin{aligned} O &= \frac{I}{I_0} \\ &= \left[ \int_0^\infty P_{sc}(\mu_{s,sc}, g_{sc}, l_{sc}) \exp(-\mu_{a,sc} l_{sc}) dl_{sc} \right] \\ &\quad \times \left[ \int_0^\infty P_e(\mu_{s,e}, g_e, l_e) \exp(-\mu_{a,m} l_e) dl_e \right] \\ &\quad \times \left[ \int_0^\infty P_d(\mu_{s,d}, g_d, l_d) \exp(-(\mu_{a,ob} + \mu_{a,db}) l_d) dl_d \right], \quad (6) \end{aligned}$$

where  $I_0$  and  $I$  are the incident and detected light intensities, respectively,  $P(\mu_s, g, l)$  is the path length probability function that depends on the scattering properties as well as on the geometry of the measurements, and  $\mu_s$ ,  $\mu_a$ ,  $g$ , and  $l$  are the scattering coefficient, the absorption coefficient, the anisotropy factor, and the photon path length, respectively. In addition, the subscripts  $m$ ,  $ob$ ,  $db$ ,  $sc$ ,  $e$ , and  $d$  indicate melanin oxygenated blood,

deoxygenated blood, the stratum corneum, epidermis, and dermis, respectively. The absorption coefficient of each chromophore is expressed as the product of its concentration  $C$  and the extinction coefficient  $\epsilon$ , i.e.,  $\mu_a = C\epsilon$ . Therefore the RGB values are expressed as functions of  $C_m$ ,  $C_{ob}$ , and  $C_{db}$ .

### 2.2 Estimation of Skin Chromophore Concentrations Based on RGB Image

Figure 1 shows the flow of estimation using the proposed method. The proposed method means a solution of the inverse problem to deduce  $C_m$ ,  $C_{ob}$ , and  $C_{db}$  from the measured RGB values. The way to solve this is by transforming the measured RGB values to XYZ values with the matrix  $N_1$  and assumes a linear relation between XYZ values and  $C_m$ ,  $C_{ob}$ , and  $C_{db}$ . The linear terms define the matrix  $N_2$ . First, RGB values in each pixel of the image are transformed into XYZ values by a matrix  $N_1$  as

$$\begin{bmatrix} X \\ Y \\ Z \end{bmatrix} = N_1 \begin{bmatrix} R \\ G \\ B \end{bmatrix}. \quad (7)$$

We determined the matrix  $N_1$  based on measurements of a standard color chart (ColorChecker, X-Rite Incorporated, Michigan) that has 24 color chips and is supplied with data for the CIEXYZ values for each chip under specific illuminations and corresponding reflectance spectra. To determine the matrix  $N_2$ , we calculated 300 diffuse reflectance spectra  $O(\lambda)$  in a wavelength range of from 400 to 700 nm at intervals of 10 nm by MCS for light transport<sup>34</sup> in skin tissue. We used the skin baseline absorption coefficient<sup>35</sup> for that of the stratum corneum. The absorption coefficient of the epidermis depends on the volume concentration of melanin in the epidermis  $C_m$ . We used the absorption coefficient of melanosome given in the literature<sup>36</sup> as the absorption coefficient of melanin  $\mu_{a,m}$ . This corresponds to the absorption coefficient of the epidermis for the case in which  $C_m = 100\%$ . We subsequently derived the absorption coefficients of the epidermis for 10 different lower concentrations of  $C_m = 1$  to 10% at intervals of 1%, by simply proportioning it to that for  $C_m = 100\%$ , and the absorption coefficients

were input for the epidermis. The sum of the absorption coefficient of oxygenated blood for  $C_{ob}$  and that of deoxygenated blood for  $C_{db}$  were considered for the dermis. This summation provides the total blood concentration  $C_{tb} = C_{ob} + C_{db}$  and oxygen saturation  $SO_2\% = (C_{ob}/C_{tb}) \times 100$ . The absorption coefficients of blood having a 44% hematocrit with 150 g/liter of hemoglobin<sup>37</sup> were assumed to be that of the dermis for the case in which  $C_{tb} = 100\%$  and were input for the dermis as  $\mu_{a,ob} + \mu_{a,db}$ . Then the absorption coefficients of the dermis were derived for five different concentrations of  $C_{tb} = 0.2, 0.4, 0.6, 0.8,$  and  $1.0\%$  for six different cases of  $SO_2 = 0, 20, 40, 60, 80,$  and  $100\%$ . Typical published values for  $\mu_s(\lambda)$ <sup>38</sup> and  $g(\lambda)$ <sup>39</sup> were input for the stratum corneum, epidermis, and dermis, which are provided as a function of wavelength. The layer thicknesses of the stratum corneum, epidermis, and dermis were set to be 0.02, 0.06, and 4.92 mm, respectively. The refractive index of the stratum corneum was set to be 1.47.<sup>40</sup> The refractive index of the epidermis was set to be 1.37, which is the average value of the volar side of the lower arm, the granular layer of the palm of the hand, and the basal layer of the palm of the hand.<sup>40</sup> The refractive index of the dermis was set to be 1.42, which is the average value of the volar side of the lower arm and the palm of the hand.<sup>40</sup> The optical parameters used in the MCS for the skin tissue model were summarized in Ref. 33. The XYZ values were then calculated based on the simulated  $O(\lambda)$ . The above calculations were performed for various combinations of  $C_m$ ,  $C_{ob}$ , and  $C_{db}$  in order to obtain the data sets of chromophore concentrations and XYZ values. Multiple regression analysis with 300 data sets established three regression equations for  $C_m$ ,  $C_{ob}$ , and  $C_{db}$ :

$$C_m = a_0 + a_1X + a_2Y + a_3Z, \quad (8)$$

$$C_{ob} = b_0 + b_1X + b_2Y + b_3Z, \quad (9)$$

$$C_{db} = c_0 + c_1X + c_2Y + c_3Z. \quad (10)$$

The regression coefficients  $a_i$ ,  $b_i$ , and  $c_i$  ( $i = 0, 1, 2, 3$ ) reflect the contributions of the XYZ values to  $C_m$ ,  $C_{ob}$ , and

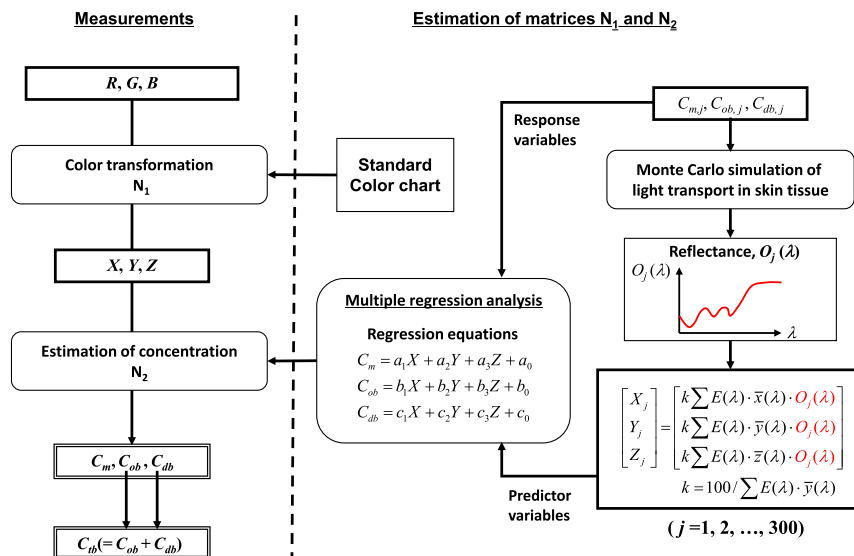


Fig. 1 Flow of estimation process for  $C_m$ ,  $C_{ob}$ ,  $C_{db}$ , and  $C_{tb}$ .

$C_{db}$ , respectively, and were used as the elements of a  $4 \times 3$  matrix  $\mathbf{N}_2$  as

$$\mathbf{N}_2 = \begin{bmatrix} a_0 & a_1 & a_2 & a_3 \\ b_0 & b_1 & b_2 & b_3 \\ c_0 & c_1 & c_2 & c_3 \end{bmatrix}. \quad (11)$$

Transformation with  $\mathbf{N}_2$  from the tristimulus values to the chromophore concentrations is thus expressed as

$$\begin{bmatrix} C_m \\ C_{ob} \\ C_{db} \end{bmatrix} = \mathbf{N}_2 \begin{bmatrix} 1 \\ X \\ Y \\ Z \end{bmatrix}. \quad (12)$$

The computation times for the MCS on obtaining all the simulated spectra and the matrix  $\mathbf{N}_2$  in Eq. (11) were 9.2 h and 10 s, respectively. Once we determine the matrices  $\mathbf{N}_1$  and  $\mathbf{N}_2$ , images of  $C_m$ ,  $C_{ob}$ , and  $C_{db}$  are reconstructed without the MCS. The total blood concentration image is simply calculated as  $C_{tb} = C_{ob} + C_{db}$ .

We perform the particular color conversion from RGB values to XYZ values for applicability of the method to different types of cameras. If the spectral sensitivity of the camera used is available, it will be possible to establish the regression equations that transform directly from RGB values to the chromophore concentrations,  $C_m$ ,  $C_{ob}$ , and  $C_{db}$  in the same manner as Eqs. (8) through (10). In such a case, however, the three regression equations for  $C_m$ ,  $C_{ob}$  and  $C_{db}$  must be prepared for every camera because each type of camera has its own spectral sensitivity. On the other hand, XYZ values are independent of types of cameras. Once we adjust the RGB responses of the camera to XYZ values by the color standard,  $C_m$ ,  $C_{ob}$ , and  $C_{db}$  can be estimated from the RGB values by only the matrix  $\mathbf{N}_2$ .

### 2.3 Calculations of Arterial Inflow, Vascular Resistance, and Venous Capacitance

The limb arterial inflow is usually determined by drawing a line on the recording of  $\Delta V/V$  mL/100 mL that is tangent to the first few seconds following the cuff inflation. The slope of this line indicates the rate of volume change, which is caused by arterial inflow.<sup>6</sup> Arterial inflow is expressed as a volume change per unit time, such as AI mL/(100 mL · min). The mean arterial pressure MAP mmHg is calculated based on the well-known standard equation

$$\text{MAP} = \text{DP} + \left( \frac{\text{SP} - \text{DP}}{3} \right), \quad (13)$$

where SP mmHg and DP mmHg are measurements of systolic pressure and diastolic pressure, respectively. Vascular resistance VR mmHg · 100 mL · min/mL can be calculated by dividing MAP by AI as

$$\text{VR} = \frac{\text{MAP}}{\text{AI}}. \quad (14)$$

Venous capacitance is defined as the percent change in volume of the limb after inflation of the occlusion cuff and can be determined by the difference between the baseline volume established prior to inflation of the cuff and the volume after the 2-min occlusion as VC mL/100 mL.<sup>6</sup>

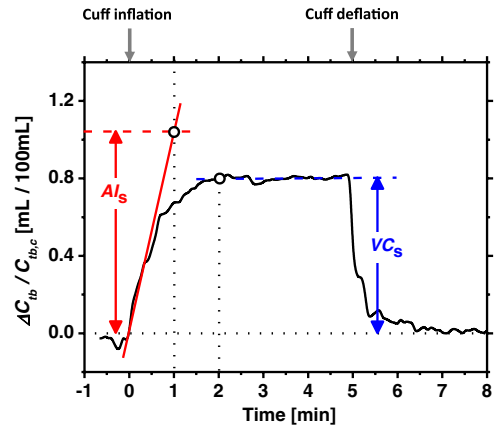


Fig. 2 Derivation of skin arterial inflow  $AI_s$  and venous capacitance  $VC_s$  from a time course of a  $\Delta C_{tb}/C_{tb,c}$  during upper arm occlusion at 50 mmHg.

Figure 2 shows an illustration of a typical response curve of skin blood volume to limb occlusion by inflation of a thigh cuff at 50 mmHg and subsequent deflation of the cuff. We calculate the arterial inflow and venous capacitance in skin as  $AI_s$  mL/(100 mL · min) and  $VC_s$  mL/100 mL, respectively, from the response curve of the change in the total blood concentration of skin  $\Delta C_{tb}/C_{tb,c}$  ( $\Delta C_{tb} = C_{tb} - C_{tb,c}$ ) to the occlusion at a pressure of 50 mmHg in the same manner as the SPG recording, where  $C_{tb,c}$  is the total blood concentration at baseline ( $t = 0$  min). Vascular resistance in skin  $VR_s$  mmHg · 100 mL · min/mL was calculated by dividing the measured MAP by  $AI_s$  (Eq. 14).

## 3 Experiments

### 3.1 Imaging System

Figure 3 schematically shows the experimental configurations for the 3(a) imaging system and 3(b) *in vivo* experiments with upper arm occlusion. A metal halide lamp (LA-180Me-R, Hayashi, Japan) illuminated the surface of a sample via a light guide with a ring illuminator. The light source covered a range from 380 to 740 nm. Diffusely reflected light was captured by a 24-bit RGB CCD camera (DFK-21BF04, Imaging Source LLC, North Carolina) and a camera lens (Pentax/Cosmica, Japan; f 16 mm, 1 : 1.4) to acquire an RGB color image of  $640 \times 480$  pixels. The field of view of the imaging system was  $360 \times 270$  mm. The lateral resolution of the images was estimated to be 0.56 mm. This indicates the best resolution with a nonscattering object. An IR-cut filter in the camera rejects unnecessary longer-wavelength light (>700 nm). A standard white diffuser with 99% reflectance (SRS-99-020, Labsphere Incorporated, North Carolina) was used to correct for the inter-instrument differences in the output of the camera and the spatial nonuniformity of the illumination. The RGB images were acquired at 15 frames per second (fps) and an average of 16 frames was stored in a personal computer at 4-s intervals and analyzed according to the visualization process described above. The standard deviation of RGB values between the 16 frames that are obtained from a subject under the normal condition was 0.15 in average, which indicate no significant difference between the 16 video frames.

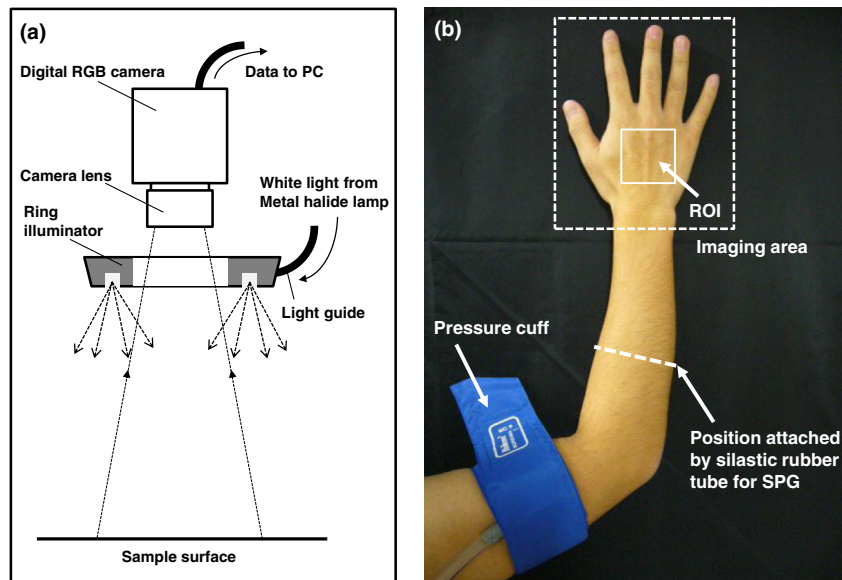


Fig. 3 Experimental configurations of (a) the imaging system and (b) the *in vivo* experiments with upper arm occlusion.

### 3.2 Upper Arm Occlusion Experiments

A pressure cuff was applied to the upper arms of 17 subjects (13 men and four women, mean age:  $23 \pm 1$  years) without any history or physical findings of venous or arterial diseases, as shown in Fig. 3(b). The five male subjects who exercised vigorously for two or more days per week and/or participated in daily physical training for at least six years were regarded as the active group (subject 1, subject 2, subject 3, subject 4, and subject 5). The remaining subjects with no or irregular physical activity (usually exercising less than one day per week) were regarded as the sedentary group. The systolic and diastolic blood pressures of the subjects were measured by the sphygmomanometer except for two of the sedentary male subjects. The data of blood pressure for the two of the sedentary male subject were unavailable owing to the experimental condition. Therefore the mean arterial blood pressure and the vascular resistance were calculated for 15 subjects in this study. The SPG (EC6, D.E. Hokanson, Washington) and a rapid cuff inflator (E-20, D.E. Hokanson) were used to measure *in vivo* forearm volume change  $\Delta V/V$  mL/100 mL. During the measurement, the subjects sat with their hands placed on a sample stage at approximately heart level. After a rest of 300 s, image acquisition and SPG recording were started and continued for 640 s at 4-s intervals. After 40 s of control, the cuff was inflated to 50 mmHg for 300 s by use of a rapid cuff inflator and subsequently deflated for 300 s. Inflation of the cuff to 50 mmHg prevents blood flow from leaving the measurement site but does not hinder arterial inflow. The SPG data was recorded for only 12 subjects whereas the acquisitions of RGB images were performed for all of the 17 subjects owing to experimental conditions. Analysis of both RGB images and forearm volume change  $\Delta V/V$  were performed offline after measurements were completed. To derive the image of  $AI_s$ , we performed the linear least squares fitting to the time course of  $\Delta C_{tb}/C_{tb,c}$  ( $t = 0-16$  s) for each pixel of a sequential image. This derivation process of  $AI_s$  image is relatively time consuming. The computation time for the images of  $AI_s$ ,  $VC_s$ , and  $VR_s$  were 1200, 7 and 1200 s, using the Intel Core 2 CPU, 2.66 GHz when the RGB color image of  $640 \times 480$  pixels was analyzed.

Use of a camera with a large number of pixels will improve the spatial resolution of resultant images, but it will increase computation time. A region of interest (ROI) was placed in a part of an image for each resultant image, as shown in Fig. 3(b). Simple linear regression analysis was used to describe the correlation coefficient  $R$  between the SPG recordings and the results obtained by the proposed method. An unpaired Student's  $t$ -test was used for statistical analysis when comparing the active group and sedentary group. The normality of the averaged value over the ROI for each group was tested by the Shapiro-Wilk test before the Student's  $t$ -test. A  $P$  value  $<0.05$  was considered statistically significant.

## 4 Results and Discussion

### 4.1 Responses of the Blood Volume to Cuff Occlusion

Figure 4 shows the forearm volume change  $\Delta V/V$  measured by the SPG for the cuff pressure of 50 mmHg and depicts differences among subjects. In Fig. 4,  $\Delta V/V$  rises quickly after the

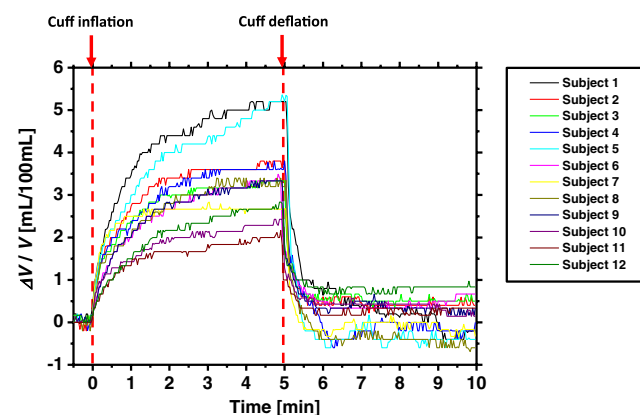


Fig. 4 Time courses of forearm volume changes  $\Delta V/V$  measured by the SPG during upper arm occlusion at 50 mmHg ( $n = 12$ ).

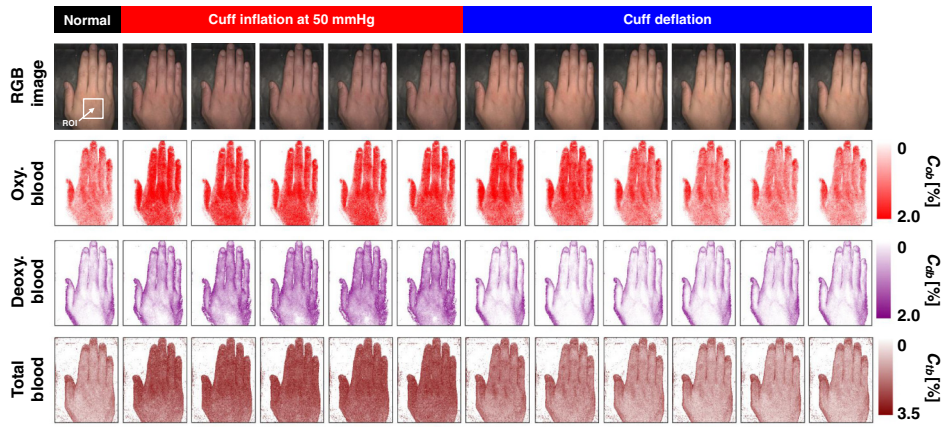


Fig. 5 Typical images of *in vivo* measurements during cuff occlusion at 50 mmHg (from top to bottom: RGB image,  $C_{ob}$ ,  $C_{db}$ , and  $C_{tb}$ ).

inflation of the cuff, and the rate of increase in  $\Delta V/V$  then slows. A rapid decrease in  $\Delta V/V$  occurred after deflation of the cuff, and  $\Delta V/V$  then returns to its baseline level. Figure 5 shows an example of the *in vivo* results obtained from one subject during cuff occlusion at 50 mmHg. The first increase in  $C_{ob}$  appeared after the cuff was inflated, which caused an increase in  $C_{tb}$ , probably due to the blockage of venous outflow and the continuous arterial inflow. After peaking,  $C_{ob}$  and  $C_{tb}$  became constant, whereas  $C_{db}$  increased during occlusion. These changes in  $C_{ob}$ ,  $C_{db}$ , and  $C_{tb}$  indicate the decrease of the arterial inflow rate and the deoxygenation of hemoglobin resulting from the consumption of oxygen by the local tissue, respectively. The rapid decreases in  $C_{ob}$ ,  $C_{db}$ , and  $C_{tb}$  immediately after the deflation of the cuff suggest the outflow of venous blood. The tendency of the response in  $C_{tb}$  to the upper arm occlusion at 50 mmHg corresponds to the results for  $\Delta V/V$  shown in Fig. 4. Although there are some artifacts due to the shade originating from the curved and irregular surfaces of the hand, the lateral distribution of  $C_{tb}$  and the response to the venous occlusion were successfully observed. Time courses of  $\Delta C_{tb}/C_{tb,c}$  averaged over the ROI corresponding to the white box in Fig. 5 are shown in Fig. 6. During the cuff occlusion,  $\Delta C_{tb}/C_{tb,c}$  increased quickly and then changed slowly. After the cuff was deflated,  $\Delta C_{tb}/C_{tb,c}$  returned immediately to the baseline levels. This tendency of variations in  $\Delta C_{tb}/C_{tb,c}$  is similar to the SPG recordings of  $\Delta V/V$  shown in Fig. 4.

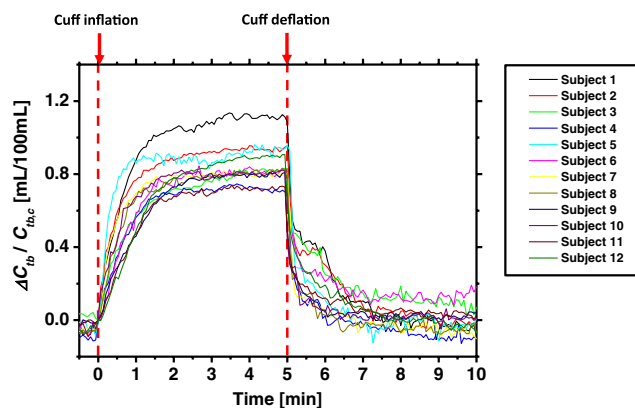


Fig. 6 Time courses of  $\Delta C_{tb}/C_{tb,c}$  averaged over the ROIs corresponding to the white box in Fig. 5 ( $n = 12$ ).

#### 4.2 Visualizations of Arterial Inflow, Vascular Resistance, and Venous Capacitance in Human Skin

Figures 7, 8, and 9 show the images of  $AI_s$ ,  $VR_s$ , and  $VC_s$ , obtained from the method, respectively. The color coded pixel values over the skin area in each image shown in Figs. 7, 8, and 9 represent the estimated values of  $AI_s$ ,  $VR_s$  and  $VC_s$ , respectively. They are used to evaluate the spatial distribution of the vasodilative indices and the differences among individuals. The average value over the area corresponding to ROI (White box) in Figs. 7, 8, and 9 is used to compare the results from the proposed method to the SPG recordings and to evaluate the difference

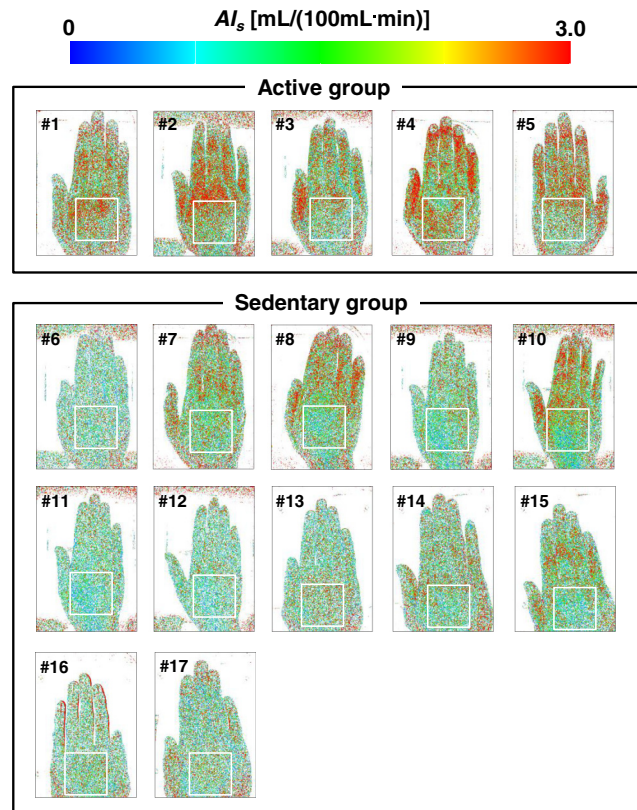
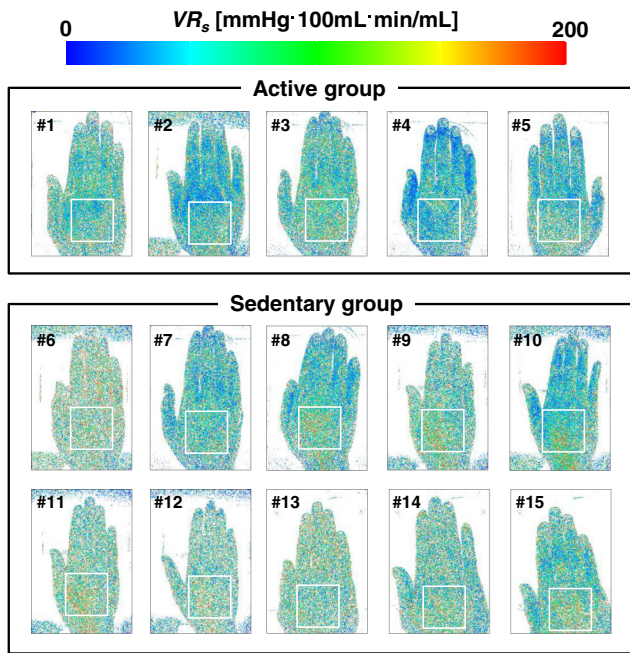


Fig. 7 Images of skin arterial inflow  $AI_s$  obtained by the proposed method ( $n = 17$ ).



**Fig. 8** Images of vascular resistance  $VR_s$  obtained by the proposed method ( $n = 15$ ).

between the active group and sedentary group. In Figs. 7, 8, and 9, it is clearly demonstrated that  $AI_s$ ,  $VR_s$ , and  $VC_s$  differ among individuals. The spatial heterogeneities can also be seen in the images of  $AI_s$ ,  $VR_s$ , and  $VC_s$ , which is indicative of spatial differences in the quantity and density of microvasculature in skin tissue. In the preliminary experiments, the repeatability of the measurements was evaluated for one subject. The results for five repeated measurements were  $0.97 \pm 0.12$  mL/100 mL · min,  $1.11 \pm 0.04$  mL/100 mL, and  $81.7 \pm 10.4$  mmHg · 100 mL · min/mL, for  $AI_s$ ,  $VC_s$ , and  $VR_s$ , respectively. We have also confirmed that the measurements are not affected by variations in the orientation of the hand.

Figure 10 shows a comparison of the results obtained from the proposed method and measurements from the SPG for 10(a) the arterial inflow, 10(b) the vascular resistance, and 10(c) the venous capacitance. The estimated  $AI_s$ ,  $VR_s$ , and  $VC_s$  are well correlated with the measurements of  $AI$ ,  $VR$ , and  $VC$  by the SPG, respectively. The correlation coefficients  $R$  between the estimated values by the method and the measurements by the SPG were calculated to be 0.83 ( $P < 0.001$ ) for the arterial inflow, 0.77 ( $P < 0.01$ ) for the vascular resistance, and 0.77 ( $P < 0.01$ ) for the venous capacitance, which revealed a significant relationship between the proposed method and measurements using the conventional SPG.

Figure 11 shows the comparison of mean values between the active group and the sedentary group for (a)  $AI_s$ , (b)  $VR_s$ , and (c)  $VC_s$ . The mean arterial inflow  $AI_s$  in the active group [ $1.50 \pm 0.29$  mL/(100 mL · min)] was significantly higher than that in the sedentary group [ $0.66 \pm 0.32$  mL/(100 mL · min)] ( $P < 0.001$ ). The mean vascular resistance  $VR_s$  in the active group ( $66.1 \pm 13.4$  mmHg · 100 mL) was significantly lower than that in the sedentary group ( $164.7 \pm 90.5$  mmHg · 100 mL · min/mL) ( $P < 0.05$ ). The mean venous capacitance  $VC_s$  in the active group ( $0.87 \pm 0.15$  mL/100 mL) was significantly higher than that in the sedentary group ( $0.69 \pm 0.14$  mL/100 mL) ( $P < 0.05$ ).

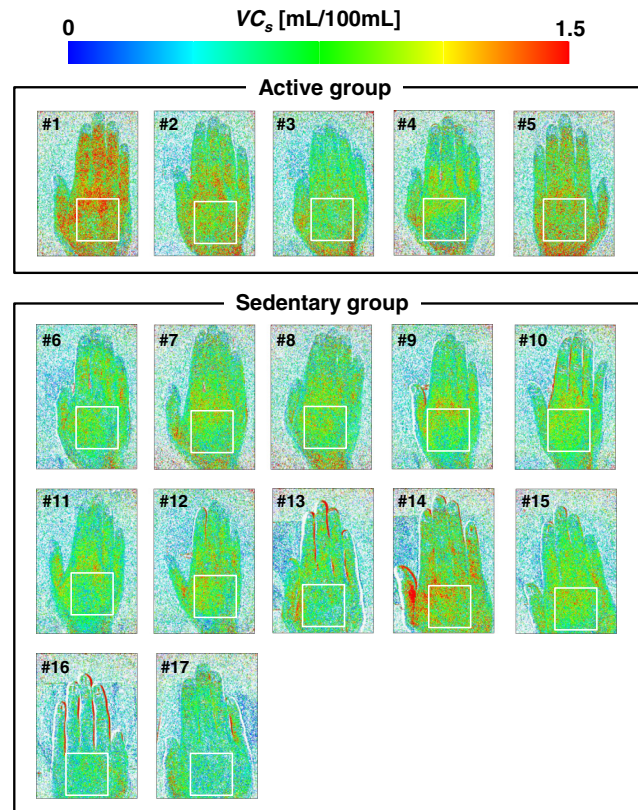


**Fig. 9** Images of venous capacitance  $VC_s$  obtained by the proposed method ( $n = 17$ ).

Previous studies have demonstrated that the peripheral vascular functions are related to the levels of physical activity and fitness.<sup>2-4</sup> It has been reported that the venous capacitance was reduced in patients with spinal cord injury compared with the able-bodied subjects, which was attributed to the combination of sympathetic denervation and the absence of regular orthostatic challenge.<sup>3</sup> Lower venous capacitance was also observed in the sedentary subjects compared with the active subjects, suggesting that the level of activity contributes to the magnitude of venous distensibility by enhancing vasodilatory responsiveness of the vessels.<sup>3</sup> The influence of physical activity on the cutaneous blood flow during leg compression has been investigated previously for the active-lifestyle subjects and the sedentary subjects.<sup>4</sup> A higher arterial inflow was demonstrated in the active subjects compared with the sedentary subjects, which was indicative of the adaptive physiologic change by the venous system to accommodate increased arterial inflow due to exercise.<sup>4</sup> A significant increase in vascular resistance in subjects with spinal cord injury was demonstrated by using the SPG recording.<sup>2</sup> The enhanced vascular resistance was discussed in terms of structural changes in vasculature, such as a decrease in the number of arterioles and capillaries and/or a decrease in the diameter of the resistance vessels as well as functional changes due to variations in endothelium-derived factors and/or sympathetic vascular regulation.<sup>2</sup> In the present study, the arterial inflow and the venous capacitance were significantly higher in the active group compared with the sedentary group, whereas the venous capacitance was significantly lower in the active group compared with the sedentary group. Therefore the differences in  $AI_s$ ,  $VR_s$ , and  $VC_s$  among individuals demonstrated in Figs. 7, 8, and 9 may reflect the variations in the level of lifestyle activity. It

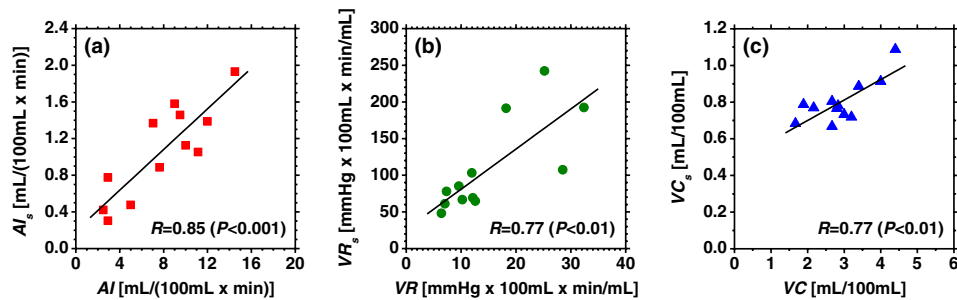


Fig. 10 Comparison of the estimated values by the proposed method and the measurements of SPG for (a) AI, (b) VR, and (c) VC ( $n = 12$ ).

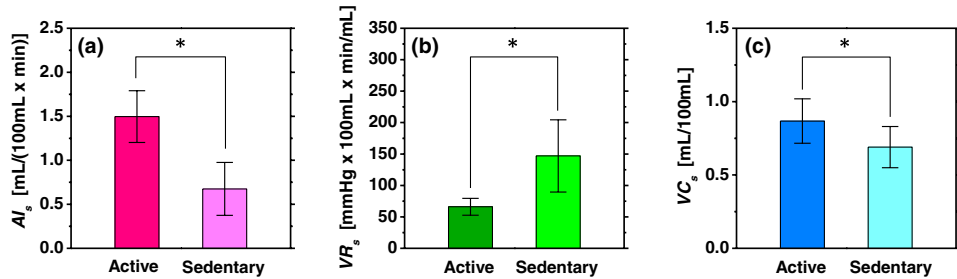


Fig. 11 Estimated values compared by subject group for (a) AI, (b) VR, and (c) VC. Values are means  $\pm$  sd. \* $P < 0.05$ .

might be possible to separate the active and sedentary groups based on the measurements of  $AI_s$ ,  $VR_s$ , and  $VC_s$  by doing discriminant analysis such as leave-one-out method. This will be useful for clinical diagnosis of various vascular dysfunctions related to the lifestyle and should be investigated in the future.

In the present study, all experiments were performed in a dark room to prevent interference from the ambient light. If the main light source is used under the ambient artificial light, the skin surface will be illuminated by the mixture of two types of lighting. In such a case, the ambient artificial light may be a source of misestimation in  $C_{ob}$ ,  $C_{db}$ , and  $C_m$ . To estimate  $C_{ob}$ ,  $C_{db}$ , and  $C_m$  accurately, the measurements of color standard for adjusting the RGB responses to XYZ values should be performed under the mixture of main light source and ambient artificial light. The ambient natural light should be avoided because it is often unreliable and variable. The RGB values of skin with darker color will be very small at very low resolution, and the conversion to XYZ color space could compound likely artifacts in measurement. In this case, the conversion from RGB color space to XYZ color space may cause misestimation of total blood  $C_{tb}$  in the dermis. Therefore, the measurements of  $AI_s$ ,  $VR_s$ , and  $VC_s$  could be affected by variations in skin color. Experiments involving individuals of African or Indian descent should be performed in the future.

## 5 Conclusions

In the present study, we proposed a method to visualize the arterial inflow, the vascular resistance, and the venous capacitance in the skin tissue from RGB digital color images. The arterial inflow and the venous capacitance in the skin tissue are successfully visualized from the increase in the rate of change in the total blood concentration and the change of the total blood concentration during upper limb occlusion at a pressure of 50 mmHg. The resultant arterial inflow with the measured mean arterial pressure also provided the image of vascular resistance in human skin. The arterial inflow, the vascular resistance,

and the venous capacitance acquired by the method were well correlated with those obtained from the conventional SPG technique. The correlation coefficients  $R$  between the estimated values by the method and the measurements by the SPG were calculated to be 0.83 ( $P < 0.001$ ) for the arterial inflow, 0.77 ( $P < 0.01$ ) for the vascular resistance, and 0.77 ( $P < 0.01$ ) for the venous capacitance. The arterial inflow and the venous capacitance in the skin tissue were significantly higher in the active group compared with the sedentary group, whereas the vascular resistance was significantly lower in the active group compared with the sedentary group. The results demonstrated in the present study imply the possibility of using the proposed method to evaluate the peripheral vascular functions in human skin. Since the proposed method visualizes both the hemodynamic response and the vasodilatory properties in skin tissue, it may be useful for evaluating the vascular function in a surgical skin flap as well as in the diagnosis of several diabetic diseases, such as peripheral neuropathy, peripheral angiopathy, and skin ulcers. We expect to further extend this method in order to investigate the vasodilatory responses in diabetic vascular diseases and endothelial dysfunction.

## Acknowledgments

Part of this work was supported by the JGC-S Scholarship foundation, Japan and by a Grant-in-Aid for Scientific Research from the Japanese Society for the Promotion of Science.

## References

1. D. H. Endemann and E. L. Schifferin, "Endothelial dysfunction," *J. Am. Soc. Nephrol.* **15**(8), 1983–1992 (2004).
2. M. T. E. Hopman et al., "Increased vascular resistance in paralyzed legs after spinal cord injury is reversible by training," *J. Appl. Physiol.* **93**(6), 1966–1972 (2002).
3. J. M. Wecht et al., "Effects of autonomic disruption and inactivity on venous vascular function," *Am. J. Physiol. Heart Circ. Physiol.* **278**(2), H515–H520 (2000).

4. A. R. Eze et al., "The contributions of arterial and venous volumes to increased cutaneous blood flow during leg compression," *Ann. Vasc. Surg.* **12**(2), 182–186 (1998).
5. A. W. Hewlett and J. G. van Zwaluwenburg, "The rate of blood flow in the arm," *Heart* **1**, 87–97 (1909).
6. R. J. Whitney, "The measurement of volume changes in human limbs," *J. Physiol.* **121**(1), 1–27 (1953).
7. L. Lind, M. Sarabi, and J. Millgard, "Methodological aspects of the evaluation of endothelium-dependent vasodilatation in the human forearm," *Clin. Physiol.* **18**(2), 81–87 (1998).
8. K. E. Cooper, O. G. Edholm, and R. F. Mottram, "The blood flow in skin and muscle of the human forearm," *J. Physiol.* **128**(2), 258–267 (1955).
9. D. E. Hokanson, D. S. Sumner, and D. E. Strandness, "An electrically calibrated plethysmograph for direct measurement of limb blood flow," *IEEE Trans. Biomed. Eng.* **BME-22**(1), 25–29 (1975).
10. J. Swampillai et al., "Review: clinical assessment of endothelial function—an update," *Br. J. Diabetes Vasc. Dis.* **5**(2), 72–76 (2005).
11. J. A. Panza et al., "Abnormal endothelium-dependent vascular relaxation in patients with essential hypertension," *N. Engl. J. Med.* **323**(1), 22–27 (1990).
12. F. Perticone et al., "Prognostic significance of endothelial dysfunction in hypertensive patients," *Circulation* **104**(2), 191–196 (2001).
13. J. E. Vigilance and H. L. Reid, "Venodynamic and hemorheological variables in patients with diabetes mellitus," *Arc. Med. Res.* **36**(5), 490–495 (2005).
14. D. J. Newton, F. Khan, and J. J. F. Belch, "Assessment of microvascular endothelial function in human skin," *Clin. Sci.* **101**(6), 567–572 (2001).
15. S. Balmain et al., "Differences in arterial compliance, microvascular function and venous capacitance between patients with heart failure and either preserved or reduced left ventricular systolic function," *Eur. J. Heart Fail.* **9**(9), 865–871 (2007).
16. J. B. Dawson et al., "A theoretical and experimental study of light absorption and scattering by *in vivo* skin," *Phys. Med. Biol.* **25**(4), 695–709 (1980).
17. J. W. Feather et al., "A portable scanning reflectance spectrophotometer using visible wavelengths for the rapid measurement of skin pigments," *Phys. Med. Biol.* **34**(7), 807–820 (1989).
18. D. K. Harrison et al., "Spectrophotometric measurements of haemoglobin saturation and concentration in skin during the tuberculin reaction in normal human subjects," *Clin. Phys. Physiol. Meas.* **13**(4), 349–363 (1992).
19. D. J. Newton et al., "Comparison of macro- and micro-lightguide spectrophotometric measurements of microvascular haemoglobin oxygenation in the tuberculin reaction in normal human skin," *Physiol. Meas.* **15**(2), 115–128 (1994).
20. A. A. Stratonnikov and V. B. Loschenov, "Evaluation of blood oxygen saturation *in vivo* from diffuse reflectance spectra," *J. Biomed. Opt.* **6**(4), 457–467 (2001).
21. G. Zonios, J. Bykowski, and N. Kollias, "Skin melanin, hemoglobin, and light scattering properties can be quantitatively assessed *in vivo* using diffuse reflectance spectroscopy," *J. Invest. Dermatol.* **117**(6), 1452–1457 (2001).
22. G. N. Stamatias and N. Kollias, "Blood stasis contributions to the perception of skin pigmentation," *J. Biomed. Opt.* **9**(2), 315–322 (2004).
23. I. Nishidate, Y. Aizu, and H. Mishina, "Estimation of melanin and hemoglobin in skin tissue using multiple regression analysis aided by Monte Carlo simulation," *J. Biomed. Opt.* **9**(4), 700–710 (2004).
24. P. R. Bargo et al., "*In vivo* determination of optical properties of normal and tumor tissue with white light reflectance and empirical light transport model during endoscopy," *J. Biomed. Opt.* **10**(3), 034018 (2005).
25. S.-H. Tseng et al., "Chromophore concentrations, absorption and scattering properties of human skin *in vivo*," *Opt. Exp.* **17**(17), 14600–14617 (2009).
26. M. G. Sowa et al., "Visible-near infrared multispectral imaging of the rat dorsal skin flap," *J. Biomed. Opt.* **4**(4), 474–481 (1999).
27. A. K. Dunn et al., "Simultaneous imaging of total cerebral hemoglobin concentration, oxygenation, and blood flow during functional activation," *Opt. Lett.* **28**(1), 28–30 (2003).
28. A. Vogel et al., "Using noninvasive multispectral imaging to quantitatively assess tissue vasculature," *J. Biomed. Opt.* **12**(5), 051604 (2007).
29. N. Tsumura, H. Haneishi, and Y. Miyake, "Independent-component analysis of skin color image," *J. Opt. Soc. Am. A* **16**(9), 2169–2176 (1999).
30. J. O'Doherty et al., "Sub-epidermal imaging using polarized light spectroscopy for assessment of skin microcirculation," *Skin Res. Tech.* **13**(4), 472–484 (2007).
31. J. O'Doherty et al., "Comparison of instrument for investigation of microcirculatory blood flow and red blood cell concentration," *J. Biomed. Opt.* **14**(3), 034025 (2009).
32. I. Nishidate et al., "Visualizing of skin chromophore concentrations by use of RGB images," *Opt. Lett.* **33**(19), 2263–2265 (2008).
33. I. Nishidate et al., "Noninvasive imaging of human skin hemodynamics using a digital red-green-blue camera," *J. Biomed. Opt.* **16**(8), 086012 (2011).
34. L.-H. Wang, S. L. Jacques, and L.-Q. Zheng, "MCML—Monte Carlo modeling of photon transport in multi-layered tissues," *Comput. Methods Programs Biomed.* **47**(2), 131–146 (1995).
35. S. L. Jacques, "Skin optics," January 1998, <http://omlc.ogi.edu/news/jan98/skinoptics.html> (30 August 2012).
36. S. L. Jacques, R. D. Glickman, and J. A. Schwartz, "Internal absorption coefficient and threshold for pulsed laser disruption of melanosomes isolated from retinal pigment epithelium," *Proc. SPIE* **2681**, 468–477 (1996).
37. S. A. Prahl, "Tabulated molar extinction coefficient for hemoglobin in water," 15 December 1999, <http://omlc.ogi.edu/spectra/hemoglobin/summary.html> (30 August 2012).
38. S. L. Jacques, "Origins of tissue optical properties in the UVA, Visible, and NIR region," in *OSA TOPS on Advances in Optical Imaging and Photon Migration*, R. R. Alfano and J. G. Fujimoto, eds., Vol. 2, pp. 364–369, Optical Society of America, Washington, DC (1996).
39. M. J. C. van Gemert et al., "Skin optics," *IEEE Trans. Biomed. Eng.* **36**(12), 1146–1154 (1989).
40. A. Knüttel and M. Boehlau-Godau, "Spatially confined and temporally resolved refractive index and scattering evaluation in human skin performed with optical coherence tomography," *J. Biomed. Opt.* **5**(1), 83–92 (2000).